THERMOMECHANICAL DEFORMATION ANALYSIS OF A TUBULAR SOLID OXIDE STEAM ELECTROLYSIS CELL

Victoria Kurushina, Vinooth Rajendran, Anil Prathuru, Mamdud Hossain, Nadimul Faisal
School of Engineering, Robert Gordon University, Aberdeen, AB10 7GJ, UK

Ajith Soman, Bahman Amini Horri, Qiong Cai
University of Surrey, University Campus, Guildford, GU2 7XH, UK

ABSTRACT

Technologies behind electrolysis cells for hydrogen production are making progress in terms of portability, cost reduction, performance enhancement, prolonged operation, and integration in stacks and with existing power infrastructure. The solid oxide steam electrolysis technology is well suited for integration with existing sources of heat and electricity given its high temperature operation. This would lead to higher efficiencies compared to other electrolyser technologies. In this study, a tubular solid oxide steam electrolysis (SOSE) cell has been investigated for high-temperature conditions. The electrolysing reaction in the SOSE occurs across a series of layers, typical composition of which comprises multiple materials (metallics, ceramics). This means significant mismatch in the thermomechanical behaviour at a high temperature which leads to the damage build up over long operation times. To analyse the combined effect of boundary conditions, material composition, porosity variation, and pressure in the internal gas channel, a series of thermomechanical simulations using finite element analysis (FEA) technique has been performed for a tubular solid oxide cell design. The results indicate significant tube elongation, which leads to stress accumulation near the fixed end connections. The maximum deformation is found to increase by about 1.4 times with the temperature elevation from 600 to 800 ^{o}C for non-porous materials. These effects can be substantially reduced if porous structures are used.

INTRODUCTION

Solid oxide steam electrolysis (SOSE) technology is developed on the intersection of applying solid materials, which exhibit specific conductivity properties in high-temperature conditions, and the conversion of both heat and electric energy into storable hydrogen fuel (Mougin 2015). Solid materials ensure the technology's portability, transportation and handling convenience, while water, as an initial substance for hydrogen production, is exceptional for its' ecological friendliness, availability, storability (Faisal, Prathuru et al. 2022). Although the SOSE can utilize a variety of feedstock materials. Recent studies related to the solid oxide electrolysis cells (SOECs) attempt to expand the range of feedstock options, advance the electrochemical efficiency, extend the lifetime of stacks and individual cells, simplify and scale fabrication, reduce costs, address challenges of integration with existing systems. Compatible systems, which can potentially benefit from the hydrogen production as a parallel process, span across several industries: nuclear energy (O'Brien, Stoots et al. 2010), renewable energy, including wind, tide, hydrothermal, solar energy sources (Karimi and Mehrpooya 2022, Wang, Wu et al. 2022,

Kasaeian, Javidmehr et al. 2023), aviation (Bradley, Droney et al. 2015, Bingaman, Holly et al. 2022, Bradley 2022), space systems (Hwang, Rho et al. 2022), and may not be limited to it (Rostami, Manshadi et al. 2022). Despite challenges, the current state of technology already proves its suitability to support the development of sustainable energy projects on planet Earth, in space and on other planetary bodies.

Solid oxide electrolysis (SOE), proton exchange membrane (PEM) electrolysis and alkaline electrolysis are three prevalent methods for splitting water to produce hydrogen (Schmidt, Gambhir et al. 2017). The SOE operates in the range of 800-1000 ^{o}C leading to higher efficiencies due to the thermodynamics of water splitting at elevated temperatures. These extreme conditions affect the choice of materials and result in durability challenges. Both PEM and alkaline electrolysis cells operate at ambient or near-ambient temperatures, up to 80 ^{o}C, a significantly lower temperature range. PEM electrolysis cells are considered to respond quickly to control signals and have excellent dynamic behaviour, coupled with a compact system design. PEM cells require expensive metal catalysts, and their durability depends on the acidic nature of the membrane. The alkaline electrolysis is currently a mature technology that involves cheaper catalyst materials and has an overall lower performance compared to PEM. Alkaline electrolysis cells are less suitable for the dynamic operation, due to a slower reaction kinetics and limitations on the mass transport in the alkaline electrolyte. The choice between these technologies depends on specific application requirements and related economic considerations. There is also currently a recognised demand for the development of SOE-based technologies and cell devices operating on an alternative basis for the temperature range from 300 ^{o}C to 600 ^{o}C, while retaining the efficiency of the hydrogen production on the level of alkaline and PEM electrolysis cells. Research in these directions will allow increasing the integrability of water electrolysis technologies and existing power infrastructures, where electricity and/or heat energy are underutilized.

Systems developed for spaceflight and challenging environments represent a very prospective niche for integration with electrolysis technologies, aiming at different operating temperatures, pressures, feedstock and resulting substances, including where conditions change rapidly. Excessive heating under direct sun rays can be accumulated as heat energy, in parallel to the use of solar arrays, and the heat can be transferred to a steam feedstock channel, directed to a stack of SOECs. This type of integration is plausible for many intermittently overheated systems, such as Earth-orbiting spacecrafts, spacecrafts on trajectories towards Venus, Mercury, Sun, where temperature differentials are greater, and permanent or temporary architectures designed for the lunar environment. In the case of water electrolysis, the output hydrogen and oxygen may be used as an extra fuel source. Additionally, SOEC represents a source of oxygen for the life support circuits in potential habitat infrastructures on Moon and Mars (Harris, Kessler et al. 2022, Choate, Harris et al. 2023, Goodliff, Merancy et al. 2023), accounting for the potential water availability in the Martian soil, and the sizes of SOEC stacks are flexible enough and could be adapted to the system's necessity.

The solid oxide technology have already been used for a number of missions in space, mainly integrated in the systems of landers, rovers and probes, supporting exploratory activities at

remote cites (Ryan, Araghi et al. 2013, Meyen, Hecht et al. 2016, Meyen 2017, Hartvigsen, Elangovan et al. 2018, Jakupca 2021, Green, Elangovan et al. 2022). Here, SOFC is used to generate electricity which can further be used for various purposes. Space exploration purposes are often linked to large variations in external conditions, so that the specific demand of the industry can be predicted to focus on the reversible SOFC/SOEC, suitable for an intermittent operation in either mode. One of well documented challenges for the use of solid oxide technology in space environments is related to isolation of the high-temperature fluids, including feedstocks, stacks of cells, storage volumes, which requires a rigor material selection and mechanical stability (Steinetz, Bansal et al. 2004, Bansal and Choi 2007, Bansal, Hurst et al. 2007).

Recent developments in the field of metamaterials, allowing a structured composition of materials at various length scales, are another dimension of progress for the improvement of solid oxide technology (Faisal, Sellami et al. 2021), including for space exploration purposes. Application of metasurfaces, layers of extreme aspect ratios, in combination with the general cell layout, material types and fabrication routes are an area of ongoing innovation, which is only possible on the intersection of disciplines. Previous works have established that one of the ways to unlock the electrolysis or fuel cell efficiency is in increasing the surface area of electrochemically active zones, while the overall cell volume and mass remain relatively similar, which is important for a payload. Metamaterials can play a great role in creating new and complex surfaces for both SOFCs and SOECs, however, the optimal recipes for the design and fabrication will be substantially different between these two.

Handling complex designs and carrying out comprehensive optimizations at the cell and stack levels can be approached by several methods and with commercially available software packages. Computational fluid dynamics (CFD), structural and thermal process analysis on their own and in multiphysics set-ups allow approaching a broad range of challenges (Li, Zhang et al. 2021). Several challenges, such as stack lifetime, material degradation and process efficiency, are often prioritized in design development as critical for the technology overall. Computational analyses for this problem are mainly based on the finite element and finite volume methods and allow both steady-state and transient simulations (Mottaghizadeh, Fardadi et al. 2021). Thermomechanical simulations here represent a specific interest, to account for the working and extreme conditions and foresee any issues with the mechanical stability of the cell. Delamination process is particularly important at the micro- and nanoscale, as the cell efficiency is closely correlated to adhesion of thin electrolyte, cathode and anode layers. Here, large deformations identified with the thermal analysis can substantially reduce the cell efficiency, hence, this is important to recognize design areas subject to deformation.

The current study aims to estimate and understand the thermomechanical deformation of the multilayer SOSE electrode subject to high temperatures, using the finite element method (FEA) based numerical calculations, to ensure mechanical stability. Analysis attempts to simulate, first, the range of intended high-temperature operating conditions, and second, to obtain estimates for some extreme combination of parameters, with a safety margin to the working conditions.

These assessments for the specific tubular design of interest will become a basis for further design iterations, involving fluid dynamics and electrochemical efficiency estimates.

The present paper is organized in four sections, where introduction provides an overall background for the role of SOEC in present and the significance of thermal analysis in the cell development. Model section is designed to outline the tubular cell model, theoretical basis of the commercial software package and the work done towards the verification of a multi-layered structure model. Results part has four subsections, where effects due to material properties and a range of operating conditions are considered. Conclusions present a summary of the thermomechanical SOEC analysis and implications to the overall cell design.

MODEL

The system considered in this paper is a single SOE tubular cell operating in the temperature range of 600-1000 ^{o}C. The SOE process is an electrochemical summary of the ion transfer, reduction and oxidation reactions, occurring at the cathode and anode layers, as shown in Fig. 1(a). The tubular cell design in this study is metal-supported, as illustrated in Fig. 1(b), which generally allows a better mechanical stability and suitable energy losses during the particle transfer, compared to alternative cathode-, electrolyte- and anode-supported designs. A full breakdown of six layers considered in the thermomechanical analysis is provided in Table 1.

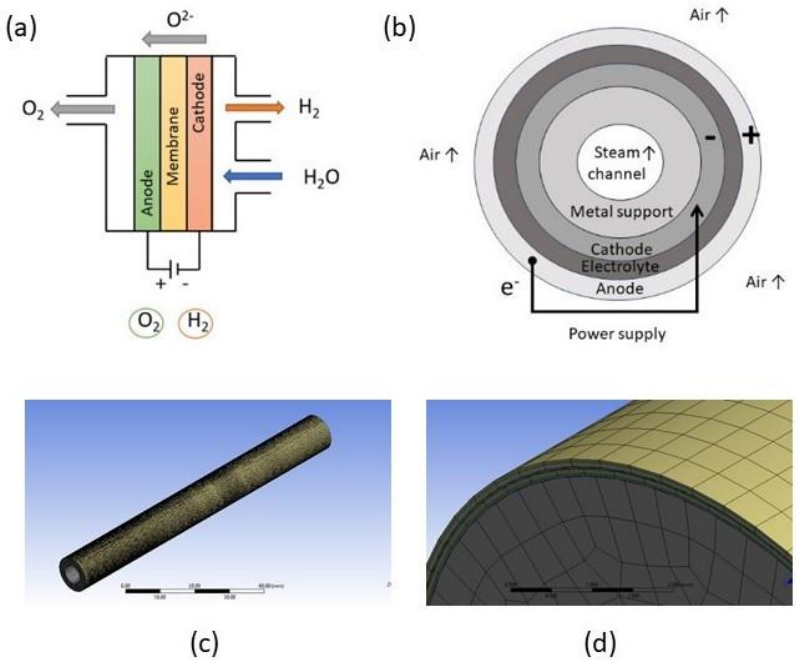

Figure 1. SOEC schematic: (a) basic electrochemistry of the solid oxide electrolysis process; (b) general view on the tubular SOEC with a thick metal support; (c) cell geometry and mesh sample to the simulation scale and (d) enlarged.

Table 1. Summary table of layers and materials

Layer	Functionality	Thickness (per design), mm	Material	Porosity (per design), %
1	Substrate (metal substrate)	2.150	Titanium alloy	30
2	Interconnect	0.035	Silver	0
3	Cathode	0.070	Nickel oxide and GDC	30
4	Electrolyte	0.022	GDC and YSZ	0
5	Anode	0.070	GDC and LSCF	30
6	Interconnect	0.035	Silver	30

The metal substrate supporting tube, the thickest layer in Fig. 1(c), of 100 mm length and 6 mm internal diameter is porous to ensure a sufficient conductivity of species towards electrochemically active cell zones. The relative proportion of thickness for the active layers, responsible for the electrolysis and hydrogen production, is demonstrated in Fig. 1(d). Here, the dense electrolyte layer is one of the most critical areas, where the low thickness allows smaller ohmic losses. This makes the thermomechanical analysis of the electrolyte layer specifically critical, because any fractures in the 0.022 mm thick structure can directly compromise the cell performance.

Properties of layers, summarized in Table 1, are incorporated in the present thermomechanical analysis in a simplified manner in the way to account for the worst-case scenario of expansion of a non-porous metal and ceramics, constrained at both ends, and expansion of the cell with an ideal designated porosity. Other simplifications include the substrate material, assumed to have properties of the alloy Ti-4V-Al, due to the high temperature data availability, and the outer interconnect layer in simulations is assumed to be a uniform porous layer, rather than an equally spaced wrapping wire.

Materials, listed in Table 1, from the intended tubular cell design include nickel oxide, gadolinia-doped ceria (GDC), yttria-stabilized zirconia (YSZ) and lanthanum strontium cobalt ferrite (LSCF), that are quite specific to the application area. For this reason, their properties for simulations are taken from the literature, as summarized in Table 2. These data are processed in order to account for the mass or volume fraction in the designed layers, mentioned in Table 1, and these materials are manually included in the material library, as specified in Table 3 per layer.

Table 2. Material properties

Material	Density, kg/m^3	Melting temperature, °C	Young's modulus, GPa	Poisson ratio	Thermal expansion coefficient, µm/m·°C	Tensile yield strength, MPa	Ultimate yield strength, MPa
Titanium alloy	**4405**	**1370**	**107**	**0.32**	**8.9**	**850**	**1098**
Silver	**10500**	**961**	**83**	**0.37**	**19**	**54**	**140**
Nickel oxide	**4670**	**1605**	**160**	**0.26**	**12.5**	**440**	**646**
GDC	**7200**	**2600**	**120**	**0.26**	**11.5**	**1.95**	**200**
YSZ	**5900**	**2700**	**210**	**0.28**	**10.5**	**750**	**1200**
LSCF	**6000**	**920**	**170**	**0.30**	**14.5**	**94**	**160**

Table 3. Properties for mixed layers incorporated in the simulation

Property	Units	Cathode	Electrolyte	Anode
Density	kg/m^3	5682	7082	6600
Melting point	°C	2003	2609	1760
Young's modulus	GPa	144	128	145
Poisson's ratio		0.26	0.26	0.28
Thermal expansion coefficient	µm/m·°C	12.1	11.4	13
Tensile yield strength	MPa	265	24.5	48
Ultimate yield strength	MPa	467	223	180

The Static Structural module of the ANSYS software generally solves the force balance with the finite element methodology, which could be presented as a matrix equation, accounting for the acting forces, stiffness matrix and displacement vector. This force balance in a steady-state at a high temperature is solved for every element with the Newton-Raphson methodology.

The numerical model for the thermomechanical analysis in this study uses standard solid body elements with three degrees-of-freedom (3DOFs) for the relatively thick substrate tube and uses

shell elements with six degrees-of-freedom (6DOFs) for the five functional layers. Shell elements in ANSYS do not account for the compression through the thickness, their formulation includes a membrane and bending behavior. The combined use of the shell and standard solid body elements in the model leads to the definition of contact regions as bonded, with the build-in Model Predictive Control (MPC) formulation.

Mesh independence test for further thermomechanical studies is performed for the 0% porosity level in all layers and fixed-fixed boundary conditions, - conditions allowing a demonstration of the worst case scenario thermal expansion of the tubular cell at all levels. The internal steam fluid channel is a source of the pressure load, acting on the internal surface of the substrate tube, with the value of 1 MPa. This is due to the laboratory experiments in the current Project planned for the pressure range of 0.5 to 1 MPa in fluid channels. The mesh independence test is conducted for the medium temperature of 800 ^{o}C in the target high temperature range, and the results are presented in Table 4. Based on these data, the grid with 90 762 elements in total for the six layers model has indicated a sufficient accuracy of the maximum total deformation estimates in the outer interconnect layer and in the inner substrate layer. This resolution is used to obtain results of the thermomechanical analysis, presented in the following section.

Table 4. Mesh independence test

#	Number of cells	Maximum total deformation of the outer silver interconnect, mm	Maximum total deformation of the titanium substrate, mm	Grid and model features' summary
1	22 537	0.10441	0.079562	Standard elements for substrate, shell elements for five functional layers, full tube of 100 mm, bonded contacts
2	37 862	0.11159	0.078981	
3	50 962	0.11234	0.078593	
4	76 192	0.11036	0.078641	
5	**90 762**	**0.088686**	**0.078468**	
6	118 342	0.094807	0.078269	
7	129 009	0.087868	0.079190	
8	141 911	0.089302	0.078229	

RESULTS

Thermomechanical results are organized in four subsections: analysis of a stress condition along the length of the 100 mm long cell; comments on the effect of the fixed boundary condition, compared to the fixed-free ends; analysis of the temperature impact, and report on the effect of porosity. These results identify the areas where the delamination, cracking and related lack of electrochemical performance can be expected, so that the tubular SOEC can be designed to avoid these conditions, including the arrangement of laboratory tests for a single cell at high

temperature conditions and the stack design, where appropriate sealing should be balanced with the cell expansion.

In order to account for the effects of porosity, properties of layer materials are modified, as given in Table 5, in a simplified manner, so that the 30% design porosity in layers 1, 3, 5 and 6 reduces these characteristics by 30%. Results for normal stresses are presented below for the selected cross-sections at 25 mm, 50 mm and 75 mm distance from one of the fixed ends of the cell. Locations of the displayed stresses are schematically shown in the cross-section in Fig. 2, so that the 0° line is consistent with the positive direction of X axis, pointing from the centre of the cross-section outwards. The line at 90° respectively corresponds to the positive direction of the Y axis.

Table 5. Properties of layers with design porosity of 30% at 20°C

Property	Units	Titanium alloy	Cathode	Anode	Silver interconnect
Density	kg/m^3	3084	3977	4620	7350
Young's modulus	GPa	74.9	101	102	58.1
Thermal expansion coefficient	µm/m·°C	6.23	8.5	9.1	13.3
Tensile yield strength	MPa	595	186	34	38
Ultimate yield strength	MPa	769	327	126	46

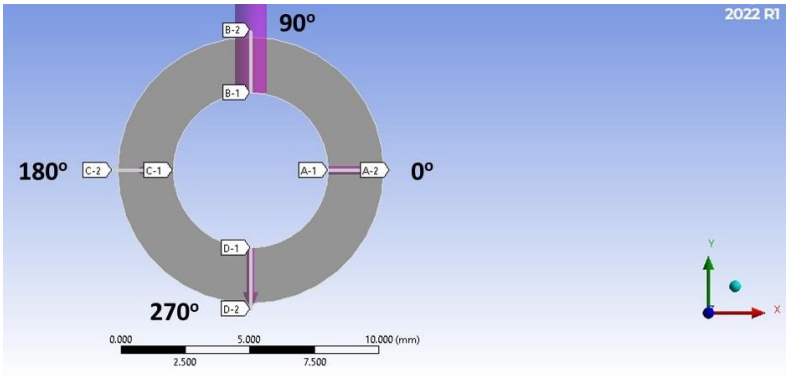

Figure 2. Geometrical locations of stresses in the cross-section.

Stress analysis of the non-porous structure at 800°C

Temperature elevation to 800°C for the SOEC leads to the deformation build up near the fixed ends and with bending effects, as seen in the contour plots in Figs 3 and 4 for each of six layers. Here, the electrolyte layer (Layer 4) has the lowest coefficient of the thermal expansion, so that the deformation of the layers below is relatively limited by the expansion of the dense electrolyte. Resulting deformation values across the tube for Layers 1-2 and Layers 3-4 are, hence, relatively similar, while Layers 5 and 6 demonstrate diverse expansions, driven by both

radial and Hoop stresses. Comparison of Figs 3 and 4 demonstrate uneven, asymmetric deformation around the tube circumference, with the maximum observed value of about 0.0887 mm.

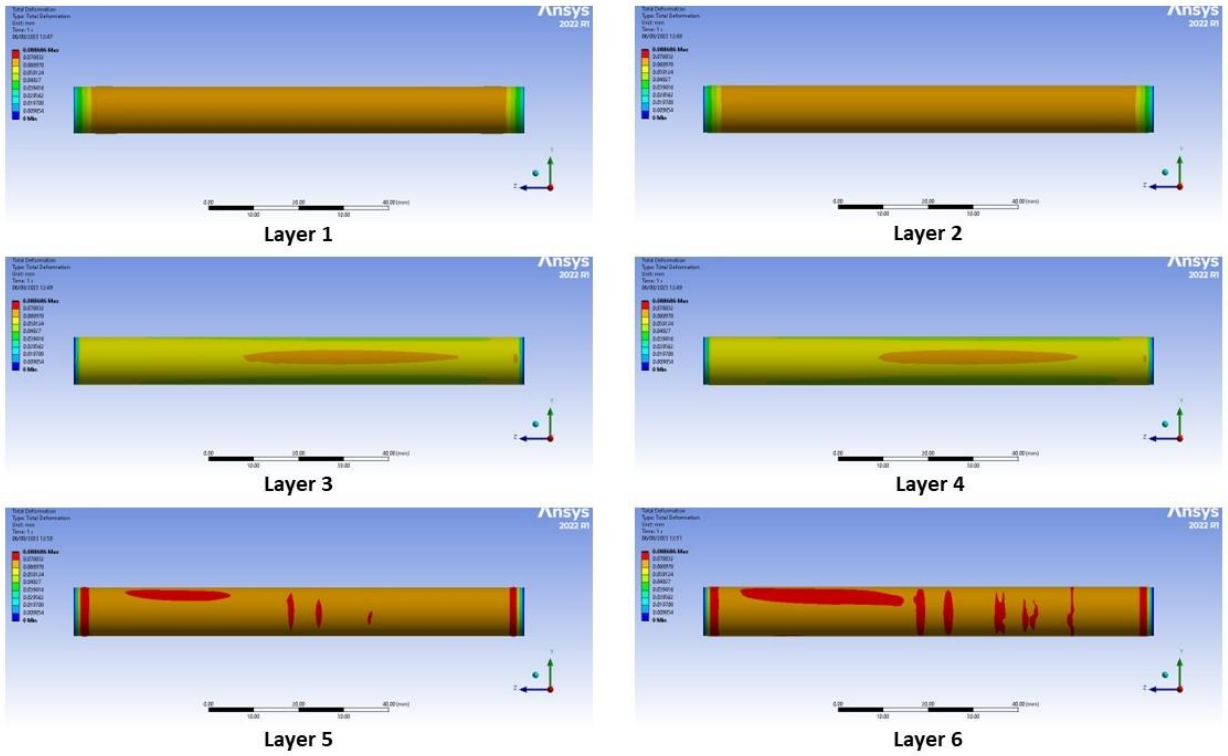

Figure 3. Contours of the total deformation in terms of six functional layers, as seen from the positive direction of the X axis, for the fixed-fixed boundary conditions and the temperature of 800°C.

Detailed view on the normal stresses in these conditions is given in Fig. 5. The figures demonstrate a limited variation of stress values for the selected locations at 0° to 270° in the cross-section, however, at least, one direction (here, at 0°) demonstrates a higher variation of the radial and Hoop stress in the substrate. In this direction, larger stresses are experienced in the cross-sections of 25 and 75 mm from the selected fixed end, compared to the middle cross-section.

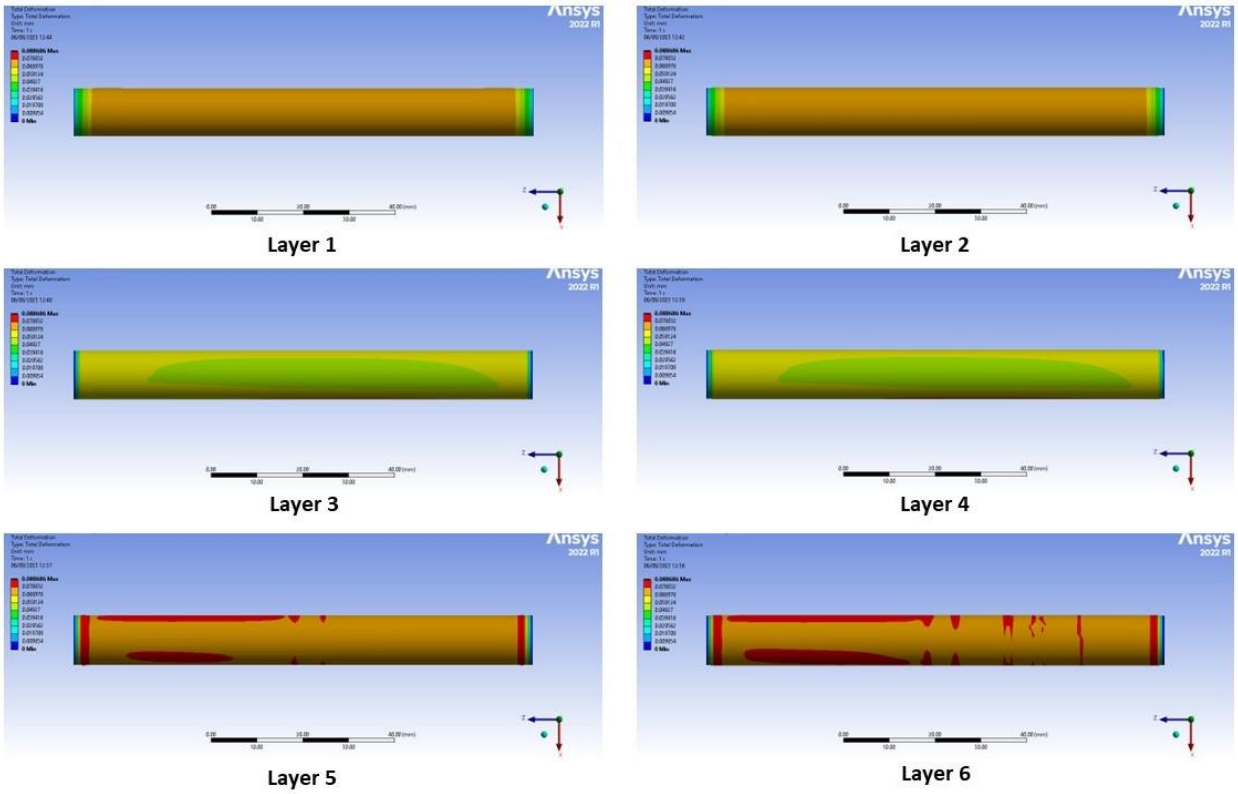

Figure 4. Contours of the total deformation in terms of six functional layers, as seen from the positive direction of the Y axis, for the fixed-fixed boundary conditions and the temperature of 800°C.

Effect of the cell constraints

Analysis of the fixed-free boundary conditions for the "worst case" non-porous structure indicates the maximum total deformation of 1.1293 mm expected at 800 °C, as shown in Fig. 6, an order of magnitude larger than any deformation seen in the fixed-fixed state. Here, functional layers expand more significantly than the metal substrate. The lower CTE of the electrolyte layer here also has some limiting effect on the resulting deformation. Thermal expansion in the direction of the free end reduces magnitude of the longitudinal stresses in the substrate and functional layers, including the difference among the layers, as illustrated in Fig. 7. These results indicate an increase in the radial stresses for all sampling locations and a relatively lower impact on Hoop stresses.

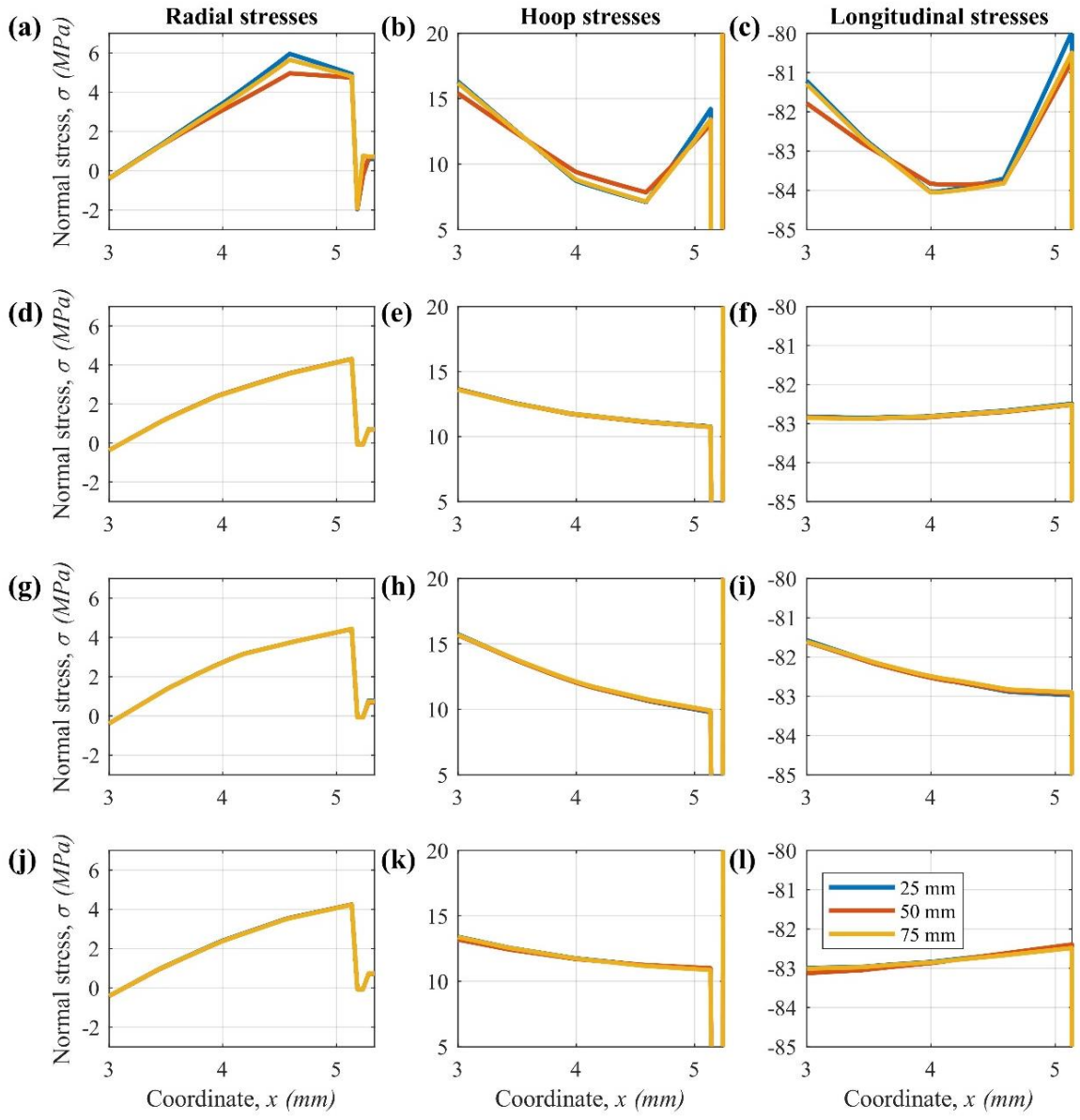

Figure 5. Variation of the normal stresses for three cross-sections along the wall coordinate with fixed-fixed boundary conditions: (a)-(c) at 0°; (d)-(f) at 90°; (g)-(i) at 180°; (j)-(l) at 270°. Here, the positive X axis direction is considered to be 0°. The view is enlarged.

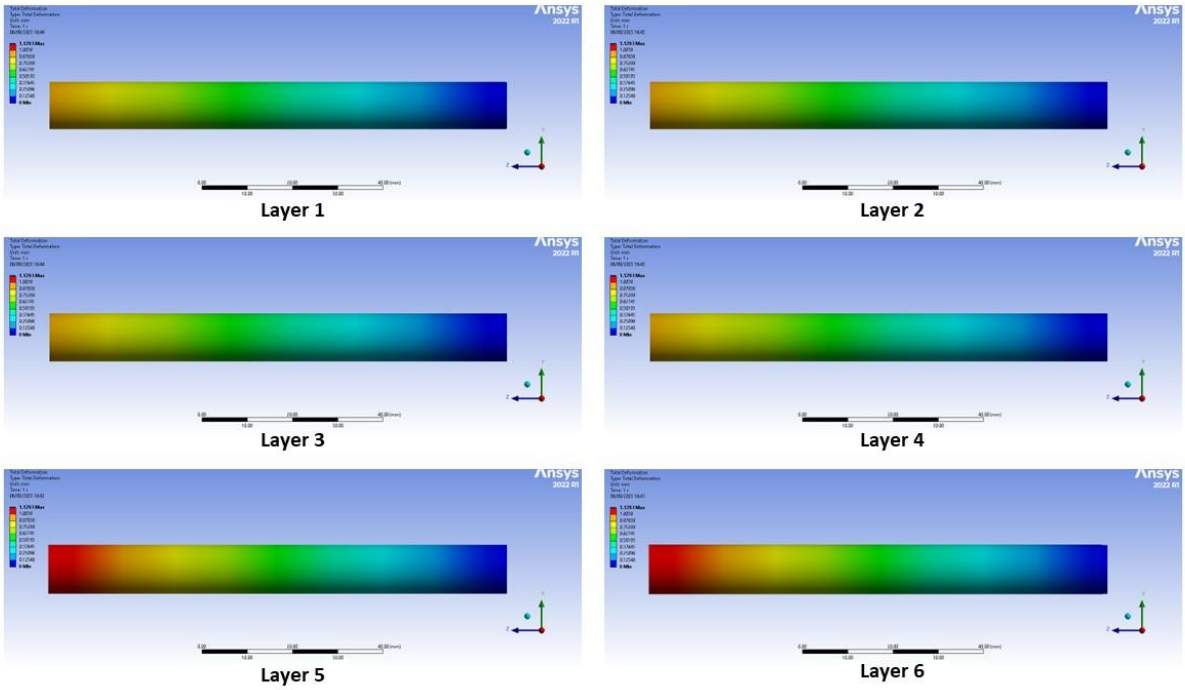

Figure 6. Contours of the total deformation in terms of six functional layers, as seen from the positive direction of the X axis, for the fixed-free boundary conditions.

High temperature effects in the SOEC model

Effect of the increasing temperature for the SOEC model with non-porous materials is shown in Fig. 8 in terms of the maximum total deformation. Here, the heating from 600 ^{o}C to 800 ^{o}C appears to be very important in building up the deformed condition, as the maximum deformation increases about 1.4 times, with the progression of this trend to the upper bound of the considered temperature range. Figure 9 illustrates the most critical deformation state in the current thermomechanical simulations at 1000 ^{o}C for the 0% porosity. As shown in this figure, the deformed condition progresses to form multiple areas of the potential crack and delamination occurrence near the fixed boundaries and in the longitudinal direction. The areas near boundaries demonstrate a relatively larger overall deformation, starting at the level of the supporting metal substrate. The outer interconnect layer additionally shows a variety of the deformed zones of a circular and elongated configuration on the sides of the cell.

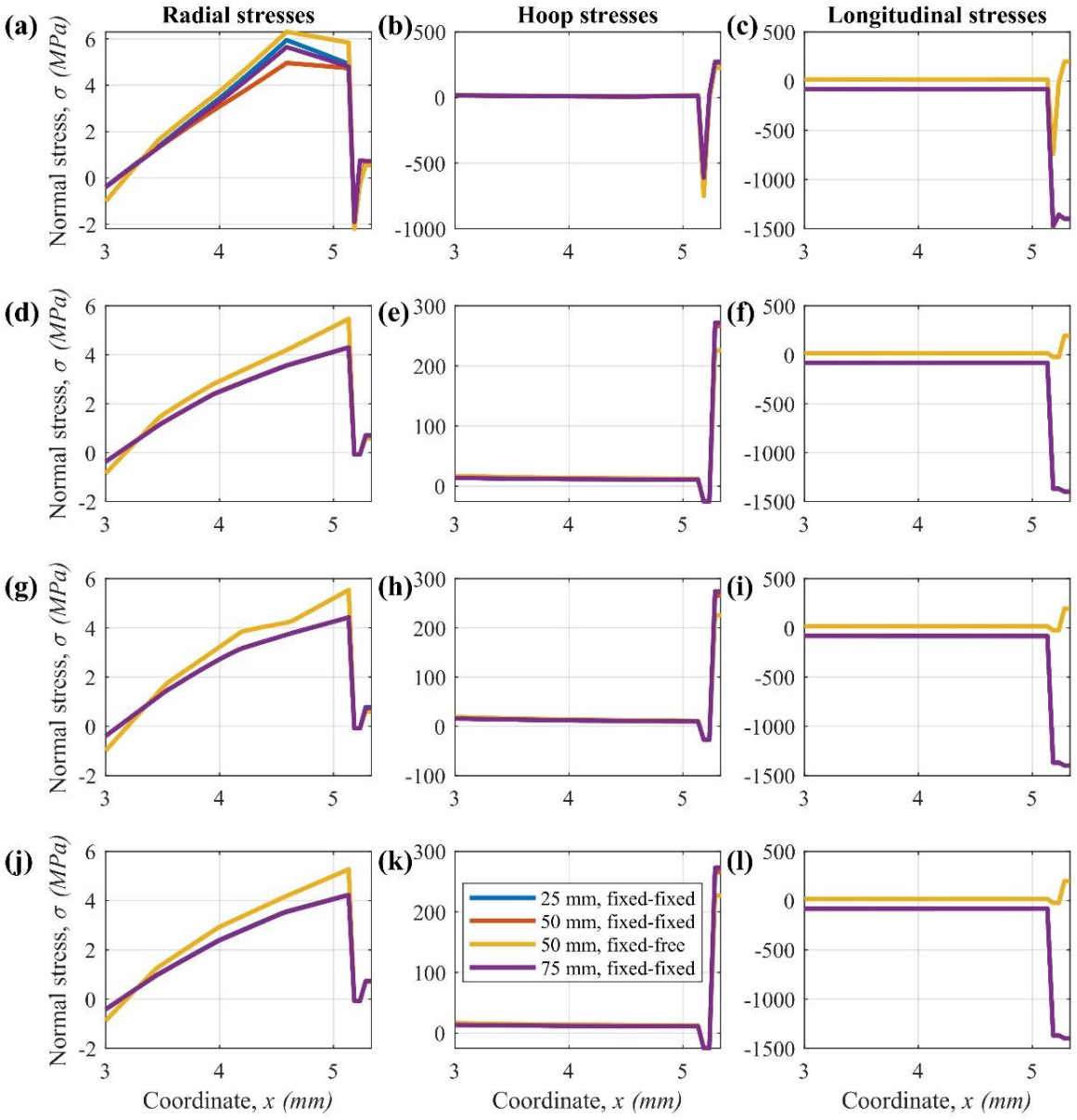

Figure 7. Comparison of the fixed-fixed and fixed-free boundary conditions in terms of the variation of normal stresses for three cross-sections along the wall coordinate: (a)-(c) at 0°; (d)-(f) at 90°; (g)-(i) at 180°; (j)-(l) at 270°. Here, the positive X axis direction is considered to be 0°. This is the full view (no scaling).

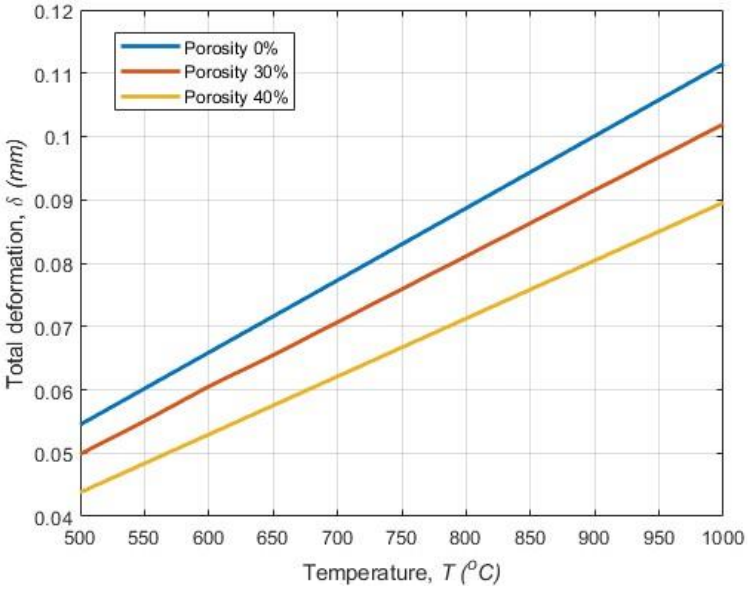

Figure 8. Maximum total deformation of the fixed-fixed porous and non-porous SOEC models in comparison, with the porous layers 1, 3, 5, 6.

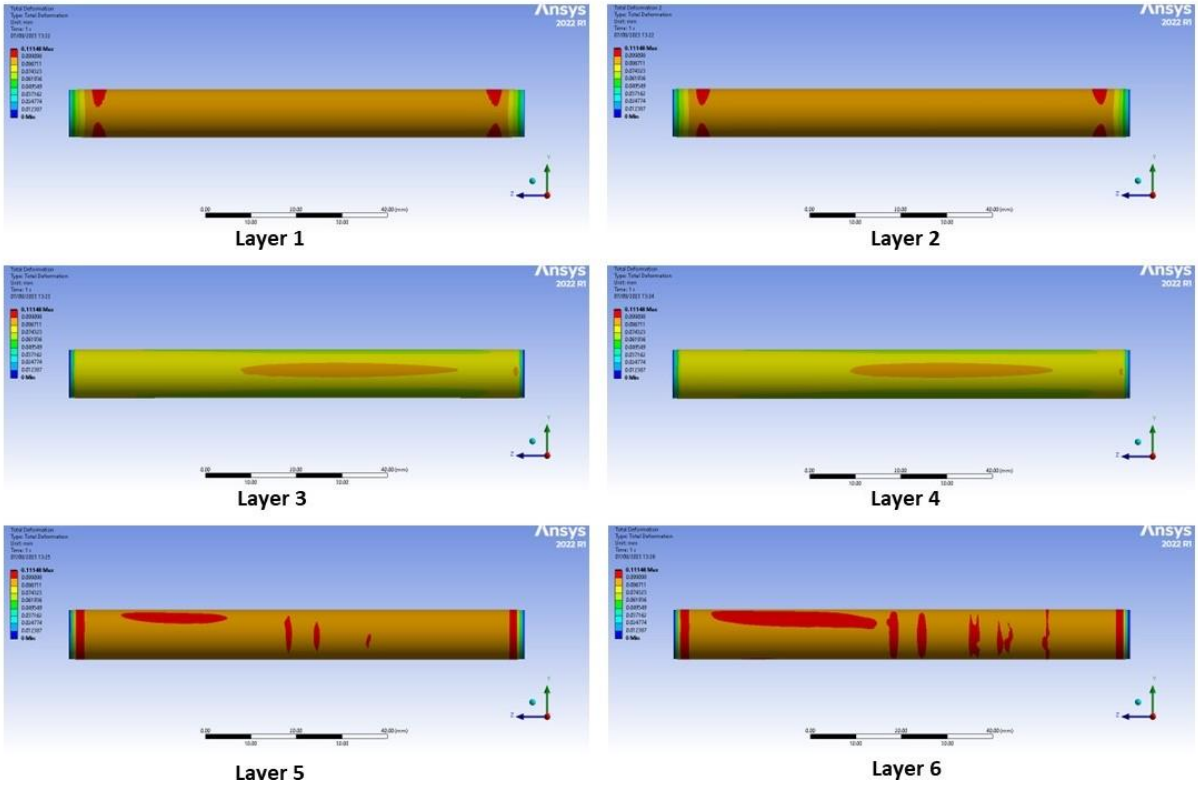

Figure 9. Contours of the total deformation of the non-porous SOEC model at 1000 °C with fixed-fixed boundaries.

Effect of porosity on the thermal expansion of the SOEC materials

Effect of porosity on the deformation of the tubular cell can be estimated based on results in Figs 8, 10, 11. Starting with the lower bound of the considered temperature range, 600 ^{o}C, implementation of the porous layers 1, 3, 5, 6, according to the proposed design, leads to a significant reduction in any observed thermal deformation, that can be quantified at the level of 10%. Figure 8 also demonstrates a significant difference between the level of expansion at the 30% and 40% porosity levels, therefore, a change to the 40% porous layers leads to another 10% reduction in the maximum total deformation. According to simulations, this pattern characterizes all the considered temperature range from 500 ^{o}C to 1000 ^{o}C.

Figures 10-11 demonstrate that the resulting deformation of porous cells at the level of the substrate and the inner silver interconnect layer is visibly concentrated around the tube bounds, while changes to the outer interconnect layer are dominated by the deformation of an elongated configuration on the sides. Compared to Figs 3, 4, 9, these contour plots indicate a lack of previously significant multiple circular shaped zones of deformation in the outer silver interconnect layer.

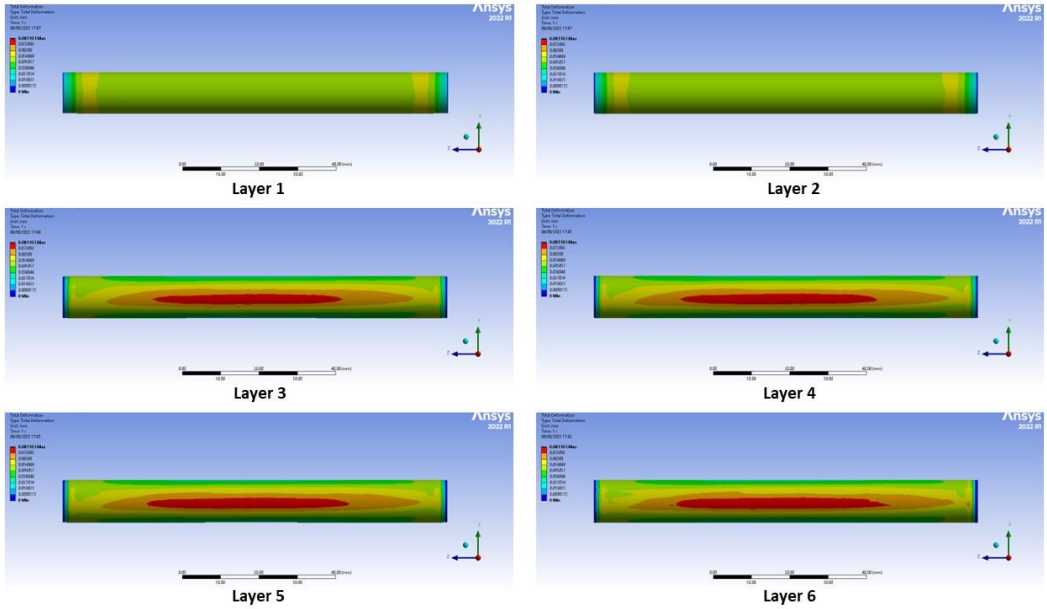

Figure 10. Contours of the total deformation of the 30% porous SOEC model at 800 ^{o}C with fixed-fixed boundaries.

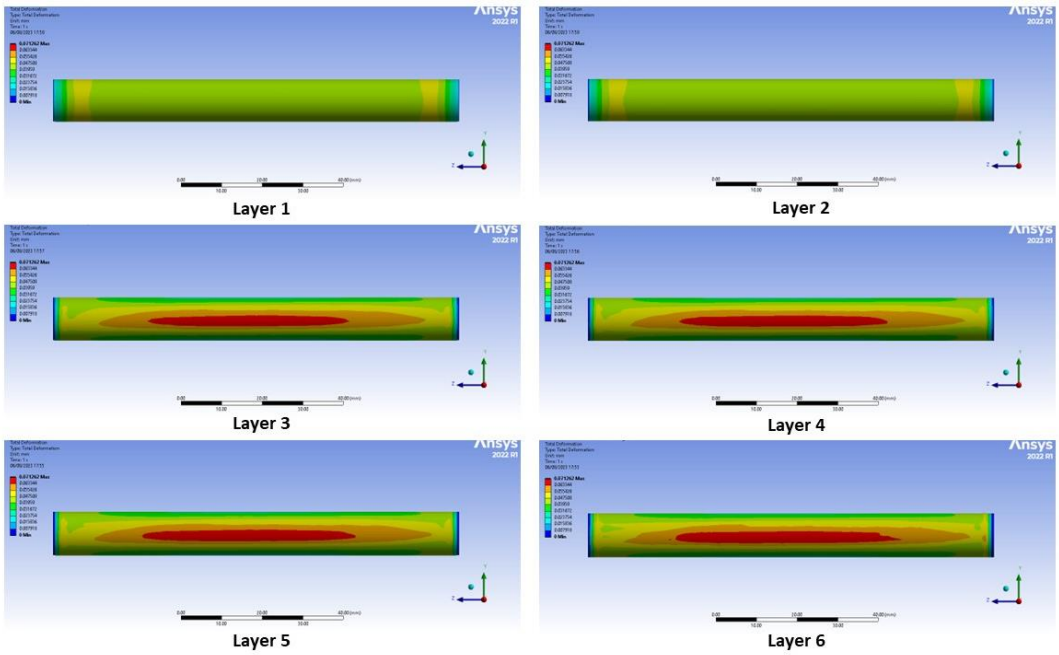

Figure 11. Contours of the total deformation of the 40% porous SOEC model at 800 ^{o}C with fixed-fixed boundaries.

CONCLUSIONS

A series of thermomechanical simulations with the high temperature deformation of the tubular SOEC model is performed in this work. Effect of the increasing temperature is estimated to be as high as about 1.4 times expansion of the non-porous model per 200 ^{o}C of heating. The thermal expansion effects become specifically pronounced above 600 ^{o}C. The porosity of 30%, apart from increasing the electrochemically active area, as proposed in the initial design for layers 1, 3, 5, 6, allows reducing the deformation at a high temperature substantially. In simulations, a further increase to the 40% porosity in the selected layers is found to allow even a more efficient reduction in the structural expansion, than raising porosity from 0% to 30%. Applying a higher level of porosity also reduces a number of circular deformed zones along the length of the cell. These results of thermomechanical simulations contribute to further improvements in the overall design of the tubular SOEC and foreseeing potential effects in the planned high temperature laboratory tests.

ACKNOWLEDGEMENTS

The authors acknowledge high temperature steam electrolysis related funding by the UKRI EPSRC via Grants No. EP/W033178/1 (METASIS). Authors (NF, AP, MH) acknowledges thermochemical electrolysis related funding by UK National Nuclear Laboratory (NNL) via gamechanger Grant No. GC 596 (THERMOSIS). Also, the author (BAH) acknowledges the funding support provided by the

Leverhulme Trust Research Fellowship (LTRF2021\17131) related to redox hydrothermal reactor for production of green hydrogen.
V.K. would like to thank Dr. Chennakesava Kadapa for the fruitful discussion on thin structures.

REFERENCES

Bansal, N. P. and S. R. Choi (2007). Glass/Ceramic Composites for Sealing Solid Oxide Fuel Cells.

Bansal, N. P., et al. (2007). Glass/BNNT Composite for Sealing Solid Oxide Fuel Cells.

Bingaman, D. C., et al. (2022). A Systems Engineering Approach for the Transition to Zero Emission Aviation. AIAA AVIATION 2022 Forum.

Bradley, M. (2022). Identification and descriptions of fuel cell architectures for aircraft applications. 2022 IEEE Transportation Electrification Conference & Expo (ITEC), IEEE.

Bradley, M. K., et al. (2015). Subsonic ultra green aircraft research.

Choate, A., et al. (2023). NASA's Moon to Mars (M2M) Transit Habitat Refinement Point of Departure Design. 2023 IEEE Aerospace Conference, IEEE.

Faisal, N. H., et al. (2022). "Application of thermal spray coatings in electrolysers for hydrogen production: advances, challenges, and opportunities." ChemNanoMat **8**(12): e202200384.

Faisal, N. H., et al. (2021). "Large-scale manufacturing route to metamaterial coatings using thermal spray techniques and their response to solar radiation." Emergent materials: 1-15.

Goodliff, K. E., et al. (2023). Exploration Systems Development Mission Directorate (ESDMD) Moon-to-Mars Architecture Definition Document, National Aeronautics and Space Administration.

Green, R. D., et al. (2022). "Perspective—solid oxide cell technology for space exploration." Journal of The Electrochemical Society **169**(5): 054528.

Harris, D. W., et al. (2022). Moon to Mars (M2M) Habitation Considerations: A Snap Shot As of January 2022.

Hartvigsen, J., et al. (2018). MOXIE development driven prospects for ISRU and atmosphere revitalization, 48th International Conference on Environmental Systems.

Hwang, M., et al. (2022). "Conceptual design and performance analysis of water electrolysis propulsion system with catalytic igniter for CubeSats." Acta Astronautica **200**: 316-328.

Jakupca, I. (2021). Update on NASA Applications using Solid Oxide Fuel Cell and Electrolysis Technologies. Ohio Fuel Cell Symposium/Solid Oxide Forum.

Karimi, M. and M. Mehrpooya (2022). "Proposal and investigation of a novel hybrid hydrogen production and liquefaction process using solid oxide electrolyzer, solar energy, and thermoelectric generator." Journal of Cleaner Production **331**: 130001.

Kasaeian, A., et al. (2023). "Integration of solid oxide fuel cells with solar energy systems: A review." Applied Thermal Engineering: 120117.

Li, Z., et al. (2021). "Advancing the multiscale understanding on solid oxide electrolysis cells via modelling approaches: A review." Renewable and Sustainable Energy Reviews **141**: 110863.

Meyen, F. E. (2017). System modeling, design, and control of the Mars Oxygen In-Situ Resource Utilization Experiment (MOXIE) and implications for atmospheric ISRU processing plants, Massachusetts Institute of Technology.

Meyen, F. E., et al. (2016). "Thermodynamic model of Mars oxygen ISRU experiment (MOXIE)." Acta Astronautica **129**: 82-87.

Mottaghizadeh, P., et al. (2021). "Dynamics and control of a thermally self-sustaining energy storage system using integrated solid oxide cells for an islanded building." International Journal of Hydrogen Energy **46**(49): 24891-24908.

Mougin, J. (2015). Hydrogen production by high-temperature steam electrolysis. Compendium of Hydrogen Energy, Elsevier**:** 225-253.

O'Brien, J., et al. (2010). High Temperature Electrolysis for Hydrogen Production from Nuclear Energy–TechnologySummary, Idaho National Lab.(INL), Idaho Falls, ID (United States).

Rostami, M., et al. (2022). "Introducing and evaluation of a new propulsion system composed of solid oxide fuel cell and downstream cycles; usage in unmanned aerial vehicles." International Journal of Hydrogen Energy **47**(28): 13693-13709.

Ryan, A. C., et al. (2013). Air-Independent Solid Oxide Fuel Cells for NASA's LOX-CH4 Landers. Fuel Cell Seminar.

Schmidt, O., et al. (2017). "Future cost and performance of water electrolysis: An expert elicitation study." International Journal of Hydrogen Energy **42**(52): 30470-30492.

Steinetz, B. M., et al. (2004). Solid Oxide Fuel Cell Seal Development at NASA Glenn Research Center. 2004 Fuel Cell Seminar.

Wang, S., et al. (2022). "Numerical assessment of a hybrid energy system based on solid oxide electrolyzer, solar energy and molten carbonate fuel cell for the generation of electrical energy and hydrogen fuel with electricity storage option." Journal of Energy Storage **54**: 105274.